

## Effect of $\text{Pb}^{2+}$ on the Luminescent Performance of Borosilicate Glass Coated $\text{CsPbBr}_3$ Perovskite Quantum Dots

YUE Zihao<sup>1,2</sup>, YANG Xiaotu<sup>1</sup>, ZHANG Zhengliang<sup>1</sup>, DENG Ruixiang<sup>1</sup>, ZHANG Tao<sup>1</sup>, SONG Lixin<sup>1,2</sup>

(1. Shanghai Institute of Ceramics, Chinese Academy of Sciences, Shanghai 200050, China; 2. School of Physical Science and Technology, ShanghaiTech University, Shanghai 201210, China)

**Abstract:** Perovskite  $\text{CsPbBr}_3$  quantum dots (PQDs) encapsulated within borosilicate glass can markedly improve their stability, expanding their applicability in sectors under lighting and display of light emitting diode (LED). However, this encapsulation has unintended consequence of reducing both the photoluminescence (PL) intensity and PL quantum yields (PLQY). This research aims to enhance the PL intensity of  $\text{CsPbBr}_3$  perovskite quantum dots glass (PQDs@glass) by exploring the effects of thermal induction temperature and  $\text{Pb}^{2+}$  content on its structural properties. The results demonstrate that the optimal thermal induction temperature for maximizing PL intensity is 460 °C, with a  $\text{Pb}^{2+}$  concentration of 6 mol. The study revealed that the increase in  $\text{Pb}^{2+}$  concentration led to the densification of the glass network structure and altered the diffusion behavior of glass components. This alteration affected the crystallization process of PQDs, which ultimately resulted in variations in the luminous intensity of PQDs@glass. This study achieved a highly desirable PLQY of 95.6% for PQDs@glass and successfully carried out size-controllable preparation of PQDs within a borosilicate glass matrix. Remarkably, the obtained results show that over 86% of the obtained PQDs particles fall within a narrow size range of 6–14 nm with average diameter of 10 nm, leading to a well-defined size distribution. Notably, these PQDs exhibit exceptional stability, as evidenced by their ability to retain an extraordinary 98.9% of the initial emission intensity following ten consecutive thermal cycles spanning from room temperature to 200 °C. Finally, to verify its applicability in LED lighting and display, the obtained PQDs@glass powder was blended with polydimethylsiloxane (PDMS), yielding exemplary LED devices which exhibit an exceptional color gamut range surpassing 110% of the standard RGB (sRGB) color space. In conclusion, this study lays the groundwork for the scalable synthesis of PQDs@glass and paves the way for its utilization in the realm of LED device technology.

**Key words:**  $\text{CsPbBr}_3$ ;  $\text{Pb}^{2+}$ ; LED; quantum dot; borosilicate glass

Light emitting diode (LED) applications in the fields of lighting and display have witnessed rapid growth alongside the progression of time and the heightening demands on its performance<sup>[1-3]</sup>.  $\text{CsPbBr}_3$  quantum dots (QDs) were considered an ideal material for LED device fabrication due to their high photoluminescence (PL) intensity, photoluminescence quantum yields (PLQY) and color purity<sup>[4-6]</sup>. However, the stability of colloidal  $\text{CsPbBr}_3$  QDs was relatively low, limiting their application in the fields of LED lighting and display. To address this issues, various strategies including ion doping<sup>[7-10]</sup>, surface passivation<sup>[11-12]</sup>, and encapsulation<sup>[13-16]</sup> were extensively explored by researchers to optimize and

enhance the stability of  $\text{CsPbBr}_3$  QDs. Although these current approaches partially improved the stability of  $\text{CsPbBr}_3$  QDs, they could only mitigate external factors' corrosion on QDs, resulting in limited protection efficacy in practical applications.

Subsequently, the strategy of encapsulating  $\text{CsPbBr}_3$  QDs in glass to form glass-ceramic was discovered by researchers, which effectively isolated  $\text{CsPbBr}_3$  QDs from the external environment and significantly enhanced their stability<sup>[17-21]</sup>, which provided an ideal solution for improving the stability of  $\text{CsPbBr}_3$  QDs. However, the use of  $\text{CsPbBr}_3$  QDs coated with glass encapsulation, displays various challenges. Firstly,

**Received date:** 2023-10-30; **Revised date:** 2023-12-05; **Published online:** 2023-12-19

**Biography:** YUE Zihao (1994–), male, Master candidate. E-mail: yuezh@shanghaitech.edu.cn

岳仔豪(1994–), 男, 硕士研究生. E-mail: yuezh@shanghaitech.edu.cn

**Corresponding author:** DENG Ruixiang. E-mail: dengruixiang@mail.sic.ac.cn; ZHANG Tao, professor. E-mail: tzhang@mail.sic.ac.cn  
邓瑞翔. E-mail: dengruixiang@mail.sic.ac.cn; 张 涛, 研究员. E-mail: tzhang@mail.sic.ac.cn

although glass is a transparent material, it inevitable scatters and refracts, attenuating the emitted light intensity and color purity of CsPbBr<sub>3</sub> QDs. Secondly, due to its amorphous nature, the internal structure of glass is complex, necessitating precise manipulation to provide an optimal environment for the formation of CsPbBr<sub>3</sub> QDs within the CsPbBr<sub>3</sub> QDs@glass system. Furthermore, the composition of CsPbBr<sub>3</sub> QDs also exerts an influence on the glass structure. An abundance of Cs promotes the formation of CsPbBr<sub>3</sub> QDs within the glass matrix. However, an excessive amount of Cs<sup>+</sup> disrupts the three-dimensional network structure of glass<sup>[22-23]</sup>. Another approach involves substituting PbBr with PbO<sup>[24]</sup>, which significantly reduces volatility during solvation, enhances the luminescent intensity of CsPbBr<sub>3</sub> QDs, and lowers production costs. Nonetheless, the higher toxicity of PbO than that of PbBr poses a challenge, and the redox implications during the melting process may cause color instability in the glass, thus detrimentally affecting the luminescent properties of CsPbBr<sub>3</sub> QDs and hindering large-scale production of CsPbBr<sub>3</sub> QDs@glass. Introducing Pb<sup>2+</sup> as an extrinsic component into the glass matrix can partially alleviate its viscosity and optimize the glass structure. However, the large radius and high charge of Pb<sup>2+</sup> exert a strong gravitational force on surrounding tetrahedral structures such as [SiO<sub>4</sub>] and [BO<sub>4</sub>]<sup>[25]</sup>, rendering the glass structure more densely packed, consequently impacting the luminescent intensity of CsPbBr<sub>3</sub> QDs. Although there is still a need for further investigation into the influence of Pb<sup>2+</sup> on the structure of CsPbBr<sub>3</sub> QDs@glass, substantial findings regarding the overall impact of Pb<sup>2+</sup> on glass have been accumulated<sup>[26-29]</sup>. Therefore, deeper understanding into the effect of Pb<sup>2+</sup> on the structure of CsPbBr<sub>3</sub> QDs@glass deserves further research.

Herein, CsPbBr<sub>3</sub> QDs@glass were fabricated employing a melt-anneal approach. Delving into the thermal induction temperature, an in-depth exploration was conducted to investigate the influence of Pb<sup>2+</sup> on the structural characteristics of CsPbBr<sub>3</sub> QDs@glass, while refining and optimizing the PL intensity of CsPbBr<sub>3</sub> QDs@glass. On this basis, the potential applications of CsPbBr<sub>3</sub> QDs@glass in the domains of LED lighting and display were systematically explored.

## 1 Experimental

### 1.1 Chemicals

Silica (SiO<sub>2</sub>, 99.95%) was purchased from Xinyi Dahan Mining Co., Ltd. Boric acid (H<sub>3</sub>BO<sub>3</sub>, 99%) was purchased from Sinopharm Chemical Reagent Co., Ltd. Zinc oxide (ZnO, 99%), calcium fluoride (CaF<sub>2</sub>), cesium

carbonate (Cs<sub>2</sub>CO<sub>3</sub>, 99%), lead bromide (PbBr<sub>2</sub>), sodium bromide (NaBr), lead oxide (PbO) were purchased from Aladdin Biochemical Technology Corp. All chemicals were used without any further purification.

### 1.2 Fabrication of CsPbBr<sub>3</sub> QDs@glass

The glass composition consists of 85SiO<sub>2</sub>-170H<sub>3</sub>BO<sub>3</sub>-55ZnO-5CaF<sub>2</sub>-16Cs<sub>2</sub>CO<sub>3</sub>-5PbBr<sub>2</sub>-15NaBr-0.5PbO. 40 g of the above raw materials were weighed and poured into a mixing tank for 2 h mixing at 25 Hz. The mixed raw materials were poured into the preheated platinum crucible, and then the lid was closed. Subsequently, all raw materials were melted in a high-temperature electric furnace at 1250 °C for 30 min. Afterward, the melted glass was poured into a preheated steel mold at 370 °C and then the molten glass was formed. Whereafter, the formed glass was returned to the muffle furnace at 370 °C for removal of stress. At this point, the precursor glass was obtained. Precursor glass was heat-treated by crystallization furnace in the range from 440 to 510 °C for 2 h. Finally, CsPbBr<sub>3</sub> QDs@glass was obtained. The preparation steps were illustrated in Fig. 1.

### 1.3 Structural characterization

X-ray diffraction system (XRD, D/max 2550 V, RIGAKU, Japan) with Cu Kα radiation (λ=0.1542 nm) was used to detect the phase structure of CsPbBr<sub>3</sub> crystals. Transmission electron microscopy (TEM, JEM-2100F, JEOL, Japan) with energy dispersive X-ray (EDX) was used to observe the microscopic morphology and size of a sample. Fourier transform infrared spectroscopy (FT-IR, EQUINOX55, Bruker, Germany) was used to test the structure of glass. X-ray photoelectron spectroscopy (XPS, Escalab250Xi, Thermo Fisher, USA) was used to test the components and change in non-bridging oxygen bonds. The samples used for testing were all in powder state.

### 1.4 Optical characterization

The PL spectra, and PLQY were recorded by a steady-state transient fluorescence spectrometer (PL, Fluorolog-3, HORIBA, Japan). The steady-state measurement system

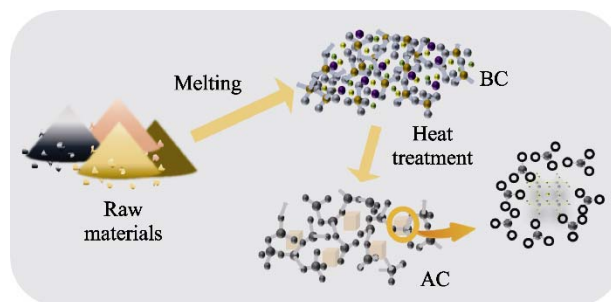


Fig. 1 Schematic of preparation of quantum dots glass-ceramics

AC: After crystallization; BC: Before crystallization

adopted a 450 W continuous Xenon lamp and CCD detector, and the transient measurement system adopted a new high-frequency pulse light source and a 980 nm pulse width continuous adjustable laser. When carrying out the spectrum test with an excitation wavelength of 365 nm, the integration time was selected as 5 s. Meanwhile, excitation light slit width was 3 nm, emission light slit width was 2 nm, and the test wavelength was in the range from 450 to 600 nm. All samples were powder state.

### 1.5 Fabrication and testing of LED device

The LED device was prepared by 2 g of polydimethylsiloxane (PDMS) with a molar ratio of  $\text{CsPbBr}_3$  QDs@glass powder, and  $n(\text{powder}) : n(\text{PDMS}) = 1 : 32$ . In order to mix evenly, the powder was magnetically stirred with PDMS for 2 h. Subsequently, the powder-glue mixture was dropped onto a 365 nm UV chip, and finally a green LED was obtained. The optical performance test of LED devices used a comprehensive optical performance characterization system (Varian, UK). During the test, a power supply with a power from 3 to 5 W was used.

## 2 Results and discussion

To investigate the influence of heat treatment on QDs microcrystalline glass and establish an optimal thermal

processing protocol for subsequent research, this study initially obtained a pristine and transparent borosilicate glass precursor under the melting conditions of 1250 °C for 30 min. Subsequently, with thermal induction time of 2 h, heat-treatment was conducted on the glass precursor, and the results for thermal induction temperatures ranging from 440 to 510 °C are shown in Fig. 2.

Fig. 2(a) exhibits the XRD patterns of  $\text{CsPbBr}_3$  QDs@glass thermal induced in temperatures ranging from 440 to 510 °C for 2 h. The data in the graph are compared with PDF#54-0752, indicating successful synthesis of  $\text{CsPbBr}_3$  QDs@glass at different temperatures. Moreover, as the temperature is elevated, the crystalline peaks become more pronounced.

Subsequently, fluorescence spectroscopy was used to characterize the samples at different temperatures, and the results are shown in Fig. 2(b-d). Fig. 2(b) depicts the PL spectra, revealing a noticeable redshift in the emission center as the temperature increasing. To investigate the underlying cause, TEM characterization was conducted, and the size distributions of  $\text{CsPbBr}_3$  QDs at different temperatures were analyzed (Fig. 3(g-k)). The results demonstrate a gradual increase in the size of  $\text{CsPbBr}_3$  QDs with the rise of temperature. At 450 °C, the QDs predominantly have a size distribution around 5 nm. In the temperature range from 460 to 490 °C, over 86% of the particles fall within the size range of 6–14 nm. When the

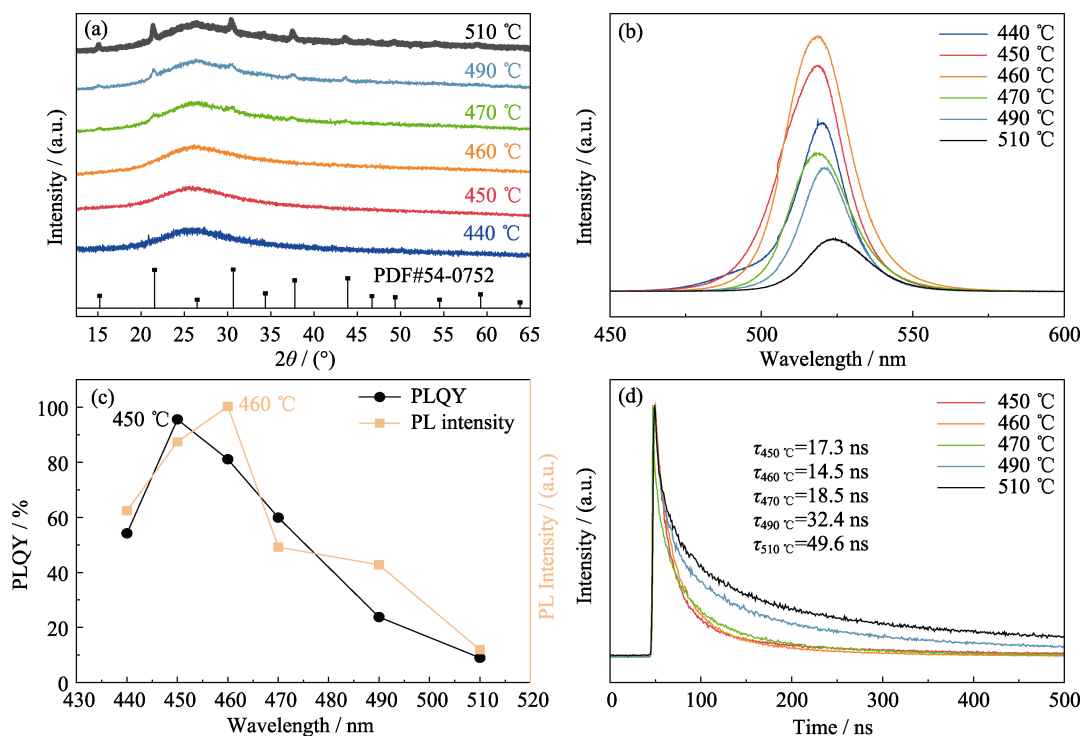


Fig. 2 Crystal structures and optical properties of PQDs@glass at different temperatures for 2 h  
(a) XRD patterns; (b) PL spectra; (c) PLQY and PL intensity; (d) Fluorescence lifetime curves

Colorful images are available on website

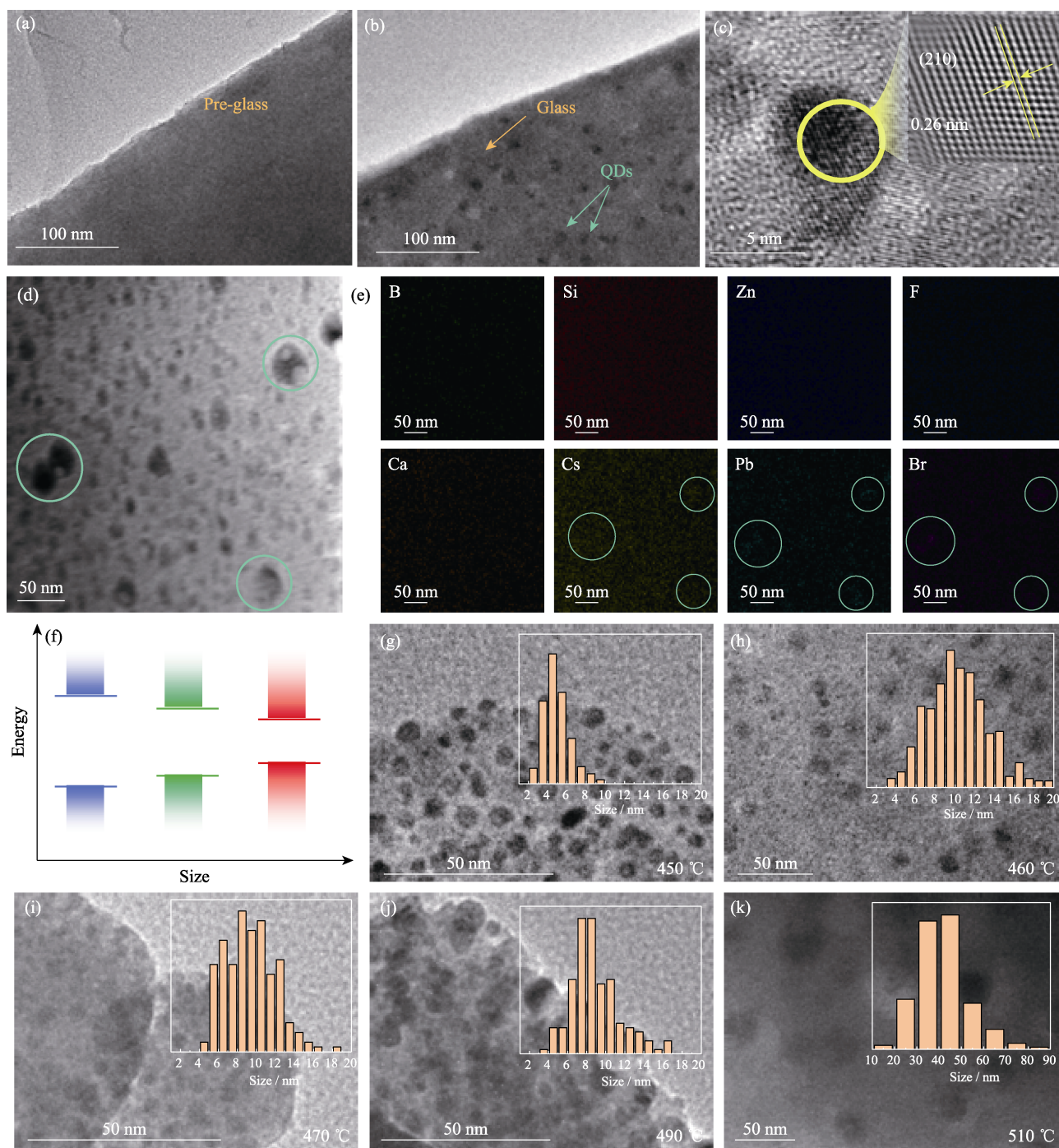


Fig. 3 TEM characterization and size distribution analyses of PQDs@glass

(a, b) TEM images before (a) and after (b) heat-treatment; (c) High-resolution TEM image; (d, e) TEM image and EDS mappings; (f) Schematic diagram of the relationship between size and band gap of CsPbBr<sub>3</sub> QDs; (g-k) TEM images and size statistics

temperature reaches 510 °C, the size distribution centers around 40 nm. This observed redshift in the emission center can be explained by the quantum size effect, where the bandgap of QDs decreases as their size increases (Fig. 3(f)).

Furthermore, the TEM images clearly indicate that the quantity of QDs increases within the temperature range from 450 to 490 °C. Initially, during the nucleation stage, the increased number of QDs leads to enhance PL intensity and PLQY. However, as the number of QDs continues to

increase, self-absorption becomes more pronounced, resulting in a decrease in PL intensity and PLQY (Fig. 2(c)). Additionally, the fluorescence spectra demonstrate that the highest PL intensity is achieved at 460 °C, while the PLQY reaches a peak value of 95.6% at 450 °C.

What follows are a further exploration of the microstructure of CsPbBr<sub>3</sub> QDs@glass, as shown in Fig. 3(a-e). Additional evidence of the successful synthesis of CsPbBr<sub>3</sub> QDs within the borosilicate glass matrix is provided by Fig. 2(a-c). Particularly, the high-resolution

TEM image (Fig. 3(c)) reveals an interlayer spacing of 0.26 nm, corresponding to the (210) crystal plane of  $\text{CsPbBr}_3$  QDs. The mapping images in Fig. 3(d, e) illustrate the accumulation of  $\text{Cs}^+$ ,  $\text{Pb}^{2+}$ , and  $\text{Br}^-$  ions within the region where the QDs precipitate. This observation aligns with previous studies suggesting that the abundance of  $\text{Cs}^+$  contributes to the formation of  $\text{CsPbBr}_3$  QDs.

With the goal of enhancing luminescence intensity, this study further investigated the influence of  $\text{Pb}^{2+}$  ions on the structure of  $\text{CsPbBr}_3$  QDs@glass, building upon the aforementioned research. The regulation of  $\text{Pb}^{2+}$  ions composition is presented in Table 1.

This resulted in a tighter glass structure and increased density.  $\text{Pb}^{2+}$  ions were able to form more bond connections within the glass network, which contributed to strengthening the three-dimensional network structure of the glass. Due to the higher charge and larger ion radius of  $\text{Pb}^{2+}$ , it exerts a strong attractive force on the surrounding  $[\text{SiO}_4]$  and  $[\text{BO}_4]$ , stabilizing the entire network structure. The decreased transparency from Pb-1 to Pb-4 further supported this observation. As a direct consequence, the glass precursor of Pb-1 formed a looser structure, facilitating the migration of  $\text{Cs}^+$ ,  $\text{Pb}^{2+}$ , and  $\text{Br}^-$  ions during annealing and stress relaxation processes, thus resulting in crystallization. With the increasing concentration of  $\text{Pb}^{2+}$  ions, the density of the glass gradually increased. However, when it exceeded a certain range, it led to the formation of more interfaces within the precursor. These interfaces lowered the energy barrier for the formation of nanocrystals by  $\text{Cs}^+$ ,  $\text{Pb}^{2+}$ , and  $\text{Br}^-$  ions. Therefore, a small portion of crystals reappeared in the precursors of Pb-3 and Pb-4.

Fig. 4(a) presents the glass precursors prepared with different conditions of  $\text{Pb}^{2+}$  ions. The results indicate

**Table 1** Component regulation of  $\text{Pb}^{2+}$  ions (all data in molar ratios)

Code	$\text{SiO}_2$	$\text{H}_3\text{BO}_3$	$\text{ZnO}$	$\text{CaF}_2$	$\text{Cs}_2\text{CO}_3$	$\text{PbBr}_2$	$\text{NaBr}$	$\text{PbO}$
Pb-1	85	170	55	5	16	4	17	0.5
Pb-2	85	170	55	5	16	5	15	0.5
Pb-3	85	170	55	5	16	6	13	0.5
Pb-4	85	170	55	5	16	7	11	0.5

that extensive crystallization did not occur in Pb-2, Pb-3, and Pb-4 precursors, whereas Pb-1 precursor exhibits crystal formation due to the larger radius of  $\text{Pb}^{2+}$  ions that occupied more space in the lattice structure and increased the atomic packing density of the glass.

The XRD results after thermal induction at 460 °C for 2 h (Fig. 4(b)) aligned with the precursor results (Fig. 4(a)). After thermal induction treatment, Pb-1 displays prominent diffraction peaks, while Pb-2, Pb-3, and Pb-4 do not. The obvious diffraction peaks in Pb-1 can be attributed to the substantial crystallization that have already occurred in its precursor (as depicted in Fig. 4(a)). Consequently, an increased number of crystals are formed during the thermal induction process, thereby resulting in the distinct diffraction peaks.

At this stage, the luminescent performance of the samples was characterized, and it was observed that Pb-3 exhibited the optimal results. This indicates that an inadequate concentration of  $\text{Pb}^{2+}$  in the precursor leads to the occurrence of uncontrollable crystallization, resulting in a reduction in the final PL intensity. Likewise, an excessive concentration of  $\text{Pb}^{2+}$  results in a high density of the borosilicate glass precursor, hindering the migration of  $\text{Cs}^+$ ,  $\text{Pb}^{2+}$ , and  $\text{Br}^-$  ions necessary for the formation of  $\text{CsPbBr}_3$  QDs. Consequently, this excessive density contributes to a decrease in PL intensity.

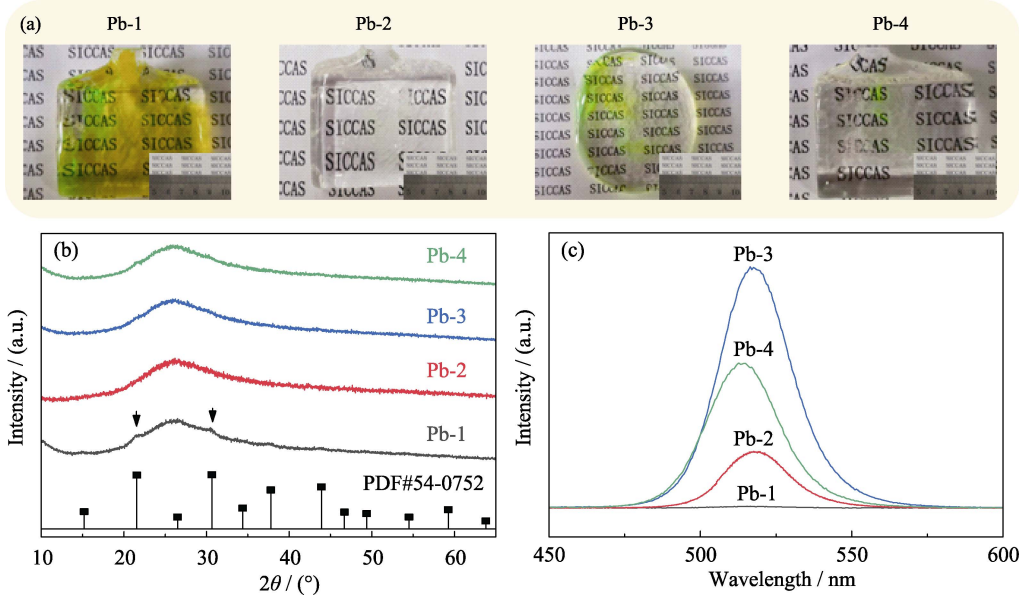


**Fig. 4** (a) Photographs, (b) XRD patterns and (c) PL spectra of  $\text{CsPbBr}_3$  QDs@glass with different  $\text{Pb}^{2+}$  concentrations

To investigate the impact of  $\text{Pb}^{2+}$  ions on the luminescent properties of  $\text{CsPbBr}_3$  QDs in glass, we further employed FT-IR and XPS to delve into the glass structure. The results are shown in Fig. 5(a-c). Fig. 5(a) illustrates that the glass network structure is primarily composed of polyhedra such as  $[\text{BO}_3]$ ,  $[\text{BO}_4]$  and  $[\text{SiO}_4]$ . The peak at  $710\text{ cm}^{-1}$  corresponds to the bending vibration of B-O bonds in the  $[\text{BO}_3]$  groups. The broad peak at  $1024\text{ cm}^{-1}$  corresponds to the stretching vibrations of both  $[\text{BO}_4]$  groups and Si-O-Si bonds. The shoulder peak at  $1272\text{ cm}^{-1}$  corresponds to the vibration of  $[\text{BO}_3]$  polyhedra, while the shoulder peak at  $1375\text{ cm}^{-1}$  corresponds to the asymmetric stretching vibration of  $[\text{BO}_3]$  polyhedra.

From Pb-1 to Pb-4, a broad peak at  $1024\text{ cm}^{-1}$  noticeably shifts towards higher wavenumber, indicating an increasing contents of  $[\text{SiO}_4]$  and  $[\text{BO}_4]$ . This suggests that the glass network structure become more compact with the increasing concentration of  $\text{Pb}^{2+}$ . It aligns well with our previous speculation regarding the occurrence of uncontrolled crystallization in the precursor. Moreover, through XPS analysis, we investigated the ratio of bridging oxygen bonds to non-bridging oxygen bonds in the borosilicate glass (Fig. 5(c)). The results indicate that the proportion of bridging oxygen bonds gradually increases as the  $\text{Pb}^{2+}$  concentration rises. This explains the aforementioned hypothesis that “ $\text{Pb}^{2+}$  exerts a

stronger attraction on neighboring  $[\text{SiO}_4]$  and  $[\text{BO}_4]$ , contributing to the enhancement of the three-dimensional network structure of the glass.”

Subsequently, this study evaluated the water resistance, UV irradiation resistance, and thermal cycling stability of the samples. The results indicate that the PL intensity can maintain over 70% of its initial value even after immersion for 360 h (Fig. 6(a)). Similarly, the PL intensity remains above 70% of its initial value after exposure to UV radiation for 210 h (Fig. 6(b)). The primary reasons for the attenuation of its water stability and UV stability are mainly due to the fact that, during the high-energy ball milling process, the powder material develops numerous cracks, resulting in a greater number of QDs being exposed. Consequently, these exposed QDs are more susceptible to environmental influences, which lead to a significant decrease in their intensity. And after undergoing 10 cycles of thermal cycling, the luminescence intensity of  $\text{CsPbBr}_3$  QDs@glass retains 98.9% of its initial value without significant decrease. The luminescence intensity for each individual cycle maintains over 80% of its initial value. Moreover, the full width at half maxima (FWHM) is relatively stable at around 24 nm, without significant change (Fig. 6(c)).

Finally, the material was mixed with PDMS and combined with a 365 nm UV chip to create LED microspheres. The characterization results (Fig. 7(a)) show that the LED

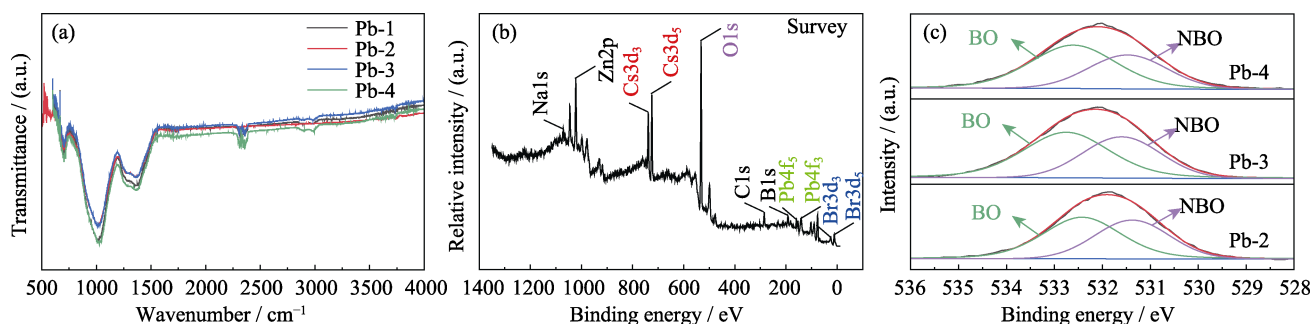


Fig. 5 Structural characterization of PQDs@glass at different  $\text{Pb}^{2+}$  concentrations

(a, b) FT-IR and XPS spectra, and (c) the ratio of bridging to non-bridging oxygen bonds; Colorful figures are available on website

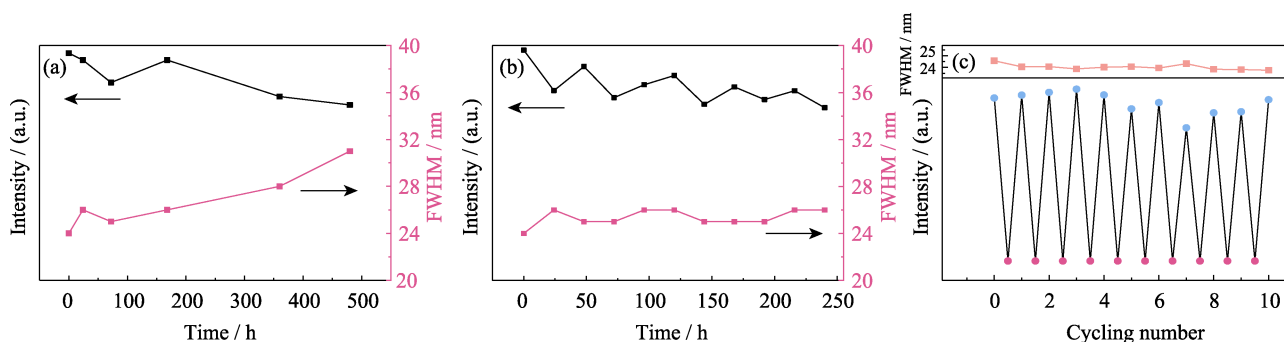


Fig. 6 Stability experiments of PQDs@glass

(a, b) Variations in PL intensity and FWHM of water resistance (a) and UV stability (b), and (c) experimental results of thermal cycling stability

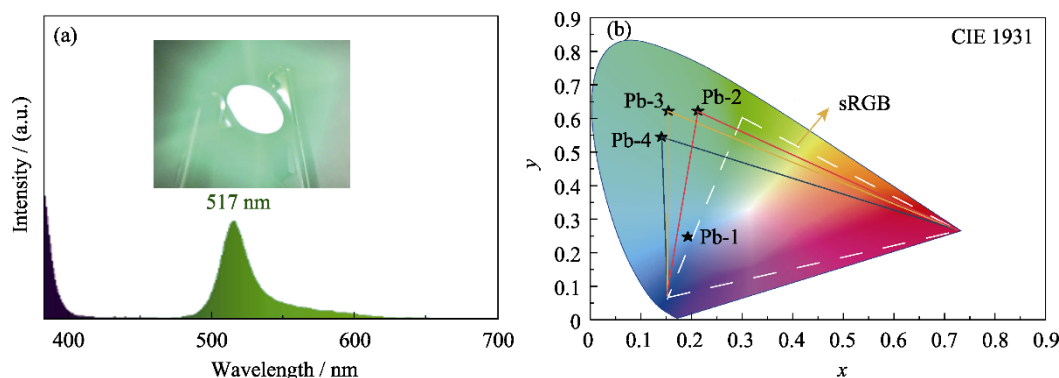


Fig. 7 (a) LED device fabricated with  $\text{CsPbBr}_3$  QDs@glass, and (b) CIE coordinates of  $\text{CsPbBr}_3$  QDs@glass LED devices at different  $\text{Pb}^{2+}$  concentrations

samples produced using Pb-2 as the base material after thermal induction at 460 °C for 2 h have an emission center at 517 nm (Fig. 2(b)), closely matching the original material's emission center at 518 nm. Additionally, Fig. 7(b) reveals that the LED color coordinates achieved with Pb-2, Pb-3, and Pb-4 are (0.21, 0.62), (0.16, 0.60) and (0.14, 0.53) respectively, encompassing a spectrum of 110% sRGB color gamut and extending the boundaries of color space.

### 3 Conclusions

In this study, we successfully prepared high-luminescence PQDs@glass under the conditions of a thermal induction temperature of 460 °C and a  $\text{Pb}^{2+}$  concentration of 6 mol. Based on this, we systematically investigated the influence of  $\text{Pb}^{2+}$  ions on the structure of PQDs@glass, and found that an increase in  $\text{Pb}^{2+}$  content leads to a densification of the microstructure of PQDs@glass, thereby affecting the diffusion of glass components and resulting in a change in the luminescence intensity of PQDs@glass. Subsequently, LED devices prepared from these materials expanded the standard RGB color gamut. This study extends the potential applications of  $\text{CsPbBr}_3$  QDs@glass in the fields of LED lighting and display, laying the foundation for the large-scale preparation of  $\text{CsPbBr}_3$  QDs@glass.

### Acknowledgements

The authors acknowledge funding sponsored by the Hengdian Group Holding Co., LTD. This research work was supported by the joint fund from Hengdian Group and Shanghai Institute of Ceramics, Chinese Academy of Sciences.

### References:

- [1] SU W, TENG Q, YUAN F. All-thermally evaporated perovskite LEDs toward high-resolution active-matrix displays. *Matter*, 2023, **6(8)**: 2539.
- [2] KIM D, PARK S, CHOI B C, *et al.* The tetravalent manganese activated  $\text{SrLaMgTaO}_6$  phosphor for w-LED applications. *Materials Research Bulletin*, 2018, **97**: 115.
- [3] CHRISTENSEN A, GRAHAM S. Thermal effects in packaging high power light emitting diode arrays. *Applied Thermal Engineering*, 2009, **29(2/3)**: 364.
- [4] WEN Z, XIE F, CHOY W C H. Stability of electroluminescent perovskite quantum dots light-emitting diode. *Nano Select*, 2021, **3(3)**: 505.
- [5] WANG S, BI C, YUAN J, *et al.* Original core-shell structure of cubic  $\text{CsPbBr}_3$ @Amorphous  $\text{CsPbBr}_x$  perovskite quantum dots with a high blue photoluminescence quantum yield of over 80%. *ACS Energy Letters*, 2017, **3(1)**: 245.
- [6] RAIN G, YAZDANI N, BOEHME S C, *et al.* Ultra-narrow room-temperature emission from single  $\text{CsPbBr}_3$  perovskite quantum dots. *Nature Communications*, 2022, **13(1)**: 2587.
- [7] ZHOU X, CHANG Q, XIANG G, *et al.* A and B sites dual substitution by  $\text{Na}^+$  and  $\text{Cu}^{2+}$  co-doping in  $\text{CsPbBr}_3$  quantum dots to achieve bright and stable blue light emitting diodes. *Spectrochimica Acta Part A: Molecular and Biomolecular Spectroscopy*, 2023, **300**: 122773.
- [8] WU W, ZHAO C, HU M, *et al.*  $\text{CsPbBr}_3$  perovskite quantum dots grown within Fe-doped zeolite X with improved stability for sensitive  $\text{NH}_3$  detection. *Nanoscale*, 2023, **15(12)**: 5705.
- [9] LIN C Q, LIU M L, YANG Z, *et al.*  $\text{Mn}^{2+}$  doped  $\text{CsPbBr}_3$  perovskite quantum dots with high quantum yield and stability for flexible array displays. *Journal of Solid State Chemistry*, 2023, **327**: 124295.
- [10] LIU S, SHAO G, DING L, *et al.* Sn-doped  $\text{CsPbBr}_3$  QDs glasses with excellent stability and optical properties for WLED. *Chemical Engineering Journal*, 2019, **361**: 937.
- [11] HUANG D, BO J, ZHENG R, *et al.* Luminescence and stability enhancement of  $\text{CsPbBr}_3$  perovskite quantum dots through surface sacrificial coating. *Advanced Optical Materials*, 2021, **9(16)**: 2100474.
- [12] ZOU L, LI X, YANG M, *et al.*  $\text{ZnPc/CsPbBr}_3$  QDs collaborative interface modification to improve the performance of  $\text{CsPbBr}_3$  perovskite solar cells. *Solar Energy Materials and Solar Cells*, 2023, **251**: 112157.
- [13] XU Y, YU L, PENG K, *et al.* Ultra-stable perovskite quantum dot composites encapsulated with mesoporous  $\text{SiO}_2$  and  $\text{PbBr}(\text{OH})$  for white light-emitting diodes. *Luminescence*, 2023, **38(5)**: 536.
- [14] REN J, LI T, ZHOU X, *et al.* Encapsulating all-inorganic perovskite quantum dots into mesoporous metal organic frameworks with significantly enhanced stability for optoelectronic applications. *Chemical Engineering Journal*, 2019, **358**: 30.

[1] SU W, TENG Q, YUAN F. All-thermally evaporated perovskite

- [15] LV W, LI L, XU M, *et al.* Improving the stability of metal halide perovskite quantum dots by encapsulation. *Advanced Materials*, 2019, **31**(28): 1900682.
- [16] LI S, NIE L, MA S, *et al.* Environmentally friendly CsPbBr<sub>3</sub> QDs multicomponent glass with super-stability for optoelectronic devices and up-converted lasing. *Journal of the European Ceramic Society*, 2020, **40**(8): 3270.
- [17] YANG B, MEI S, ZHU Y, *et al.* Precipitation promotion of highly emissive and stable CsPbX<sub>3</sub> (Cl, Br, I) perovskite quantum dots in borosilicate glass with alkaline earth modification. *Ceramics International*, 2023, **49**(4): 6720.
- [18] TONG Y, WANG Q, LIU X, *et al.* The promotion of TiO<sub>2</sub> induction for finely tunable self-crystallized CsPbX<sub>3</sub> (X = Cl, Br and I) nanocrystal glasses for LED backlighting display. *Chemical Engineering Journal*, 2022, **429**: 132391.
- [19] SHAO G, LIU S, DING L, *et al.* K<sub>x</sub>Cs<sub>1-x</sub>PbBr<sub>3</sub> NCs glasses possessing super optical properties and stability for white light emitting diodes. *Chemical Engineering Journal*, 2019, **375**: 122031.
- [20] LIU S, HE M, DI X, *et al.* Precipitation and tunable emission of cesium lead halide perovskites (CsPbX<sub>3</sub>, X = Br, I) QDs in borosilicate glass. *Ceramics International*, 2018, **44**(4): 4496.
- [21] LIU J, SHEN L, CHEN Y, *et al.* Highly luminescent and ultrastable cesium lead halide perovskite nanocrystal glass for plant-growth lighting engineering. *Journal of Materials Chemistry C*, 2019, **7**(43): 13606.
- [22] STOCH P, STOCH A. Structure and properties of Cs containing borosilicate glasses studied by molecular dynamics simulations. *Journal of Non-Crystalline Solids*, 2015, **411**: 106.
- [23] LIU Q, FENG L, SUN Y, *et al.* Effects of phosphate glass on Cs<sup>+</sup> immobilization in geopolymer glass-ceramics. *Ceramics International*, 2023, **49**(4): 6545.
- [24] YANG B, MEI S, HE H, *et al.* Lead oxide enables lead volatilization pollution inhibition and phase purity modulation in perovskite quantum dots embedded borosilicate glass. *Journal of the European Ceramic Society*, 2022, **42**(1): 258.
- [25] KAUR N, KHANNA A, G NZ LEZ-BARRIUSO M, *et al.* Effects of Al<sup>3+</sup>, W<sup>6+</sup>, Nb<sup>5+</sup> and Pb<sup>2+</sup> on the structure and properties of borotellurite glasses. *Journal of Non-Crystalline Solids*, 2015, **429**: 153.
- [26] OTHMAN H, TOPPER B, ELKHOLY H, *et al.* Structural, spectroscopic, and radiation shielding properties of Pb<sup>2+</sup>-doped borate and phosphate glasses. *International Journal of Applied Glass Science*, 2023, **14**(3): 408.
- [27] LI P, TIAN Y, HUANG F, *et al.* Highly efficient photostimulated luminescence of Pb<sup>2+</sup>-doped SrAl<sub>2</sub>O<sub>4</sub>:Eu<sup>2+</sup>, Dy<sup>3+</sup> borate glass for long-term stable optical information storage. *Journal of the European Ceramic Society*, 2022, **42**(12): 5065.
- [28] EL-EGILI K, DOWEIDAR H, MOUSTAFA Y M, *et al.* Structure and some physical properties of PbO-P<sub>2</sub>O<sub>5</sub> glasses. *Physica B: Condensed Matter*, 2003, **339**(4): 237.
- [29] CHENG Y, XIAO H, GUO W, *et al.* Structure and crystallization kinetics of PbO-B<sub>2</sub>O<sub>3</sub> glasses. *Ceramics International*, 2007, **33**(7): 1341.

## Pb<sup>2+</sup>对掺杂硼硅酸盐玻璃中 CsPbBr<sub>3</sub> 钙钛矿量子点发光性能的影响

岳仔豪<sup>1,2</sup>, 杨小兔<sup>1</sup>, 张正亮<sup>1</sup>, 邓瑞翔<sup>1</sup>, 张涛<sup>1</sup>, 宋力昕<sup>1,2</sup>

(1. 中国科学院 上海硅酸盐研究所, 上海 200050; 2. 上海科技大学 物质科学与技术学院, 上海 201210)

**摘要:** 硼硅酸盐玻璃包覆钙钛矿 CsPbBr<sub>3</sub> 量子点(PQDs@glass)能够大幅提高 PQDs 的稳定性, 使其在 LED 照明和显示技术中拥有广泛的应用空间。然而, 玻璃包覆的同时也导致了 PQDs 发光强度与量子产率降低。本工作为提高其发光强度探讨了热诱导温度及 Pb<sup>2+</sup> 的含量对 PQDs@glass 结构的影响, 当热诱导温度为 460 °C, Pb<sup>2+</sup> 浓度为 6 mol 时, 其发光强度最高。研究发现, Pb<sup>2+</sup> 浓度的增加会导致玻璃网状结构的致密化, 改变玻璃组分的扩散行为, 影响 PQDs 的析晶过程, 导致 PQDs@glass 发光强度的变化。本工作得到量子产率高达 95.6% 的 PQDs@glass, 并实现了硼硅酸盐玻璃基质内 PQDs 的尺寸可控制备。结果表明, PQDs 尺寸分布在 10 nm 左右, 超过 86% 的颗粒尺寸在 6~14 nm 内, 且具有优越的稳定性, 经历 10 次室温至 200 °C 热循环后, 发光强度仍能保持初始强度的 98.9%。最后, 为了验证其在 LED 照明及显示领域的应用, 将制备的量子点微晶玻璃粉料与二甲硅氧烷(PDMS)混合, 得到的 LED 器件性能优异, 色域范围覆盖 110% sRGB。本研究为 PQDs@glass 的大规模制备及其在 LED 器件领域的应用奠定了基础。

**关键词:** CsPbBr<sub>3</sub>; Pb<sup>2+</sup>; LED; 量子点; 硼硅酸盐玻璃

中图分类号: TQ174 文献标志码: A 文章编号: 1000-324X(2024)04-0449-08